THE ASTROPHYSICAL JOURNAL, 421:585–599, 1994 February 1

Al III, Si IV, AND C IV ABSORPTION TOWARD ζ OPHIUCHI: EVIDENCE FOR PHOTOIONIZED AND COLLISIONALLY IONIZED GAS[1]

KENNETH R. SEMBACH,[2] BLAIR D. SAVAGE,[3] AND EDWARD B. JENKINS[4]
Received 1993 April 26; accepted 1993 August 6

ABSTRACT

We present Goddard High-Resolution Spectrograph observations at 3.5 km s^{-1} resolution and signal-to-noise ratios of 30 to 60 for the Al III, Si IV, C IV, and N V absorption lines in the far-ultraviolet spectrum of the O9.5 V star ζ Ophiuchi. The measurement reveal three types of highly ionized gas along the 140 pc line of sight.

1. Narrow components of Al III ($b = 4.3$ km s^{-1}, $\langle v_{\rm helio} \rangle = -7.8$ km s^{-1}; $b = 3.2$ km s^{-1}, $\langle v_{\rm helio} \rangle = -14.4$ km s^{-1}) and Si IV ($b = 5.3$ km s^{-1}, $\langle v_{\rm helio} \rangle = -15.0$ km s^{-1}) trace photoionized gas in the expanding H II region surrounding ζ Oph. The observed magnitude and direction of the velocity offset between the Al III and Si IV profiles can be explained by models of H II regions that incorporate expansion. Narrow C IV absorption associated with the H II region is not detected. Predictions of the expected amounts of Si IV and C IV overestimate the column densities of these ions by factors of 30 and more than 10, respectively. The discrepancy may be due to the effects of elemental depletions in the gas and/or to the interaction of the stellar wind with surrounding matter.

2. Broad ($b = 15$ to 18 km s^{-1}) and weak Si IV and C IV absorption components are detected near $\langle v_{\rm helio} \rangle = -26$ km s^{-1}. The high-ionization species associated with these absorption components are probably produced by electron collisional ionization in a heated gas. This absorption may be physically related to the ζ Oph bow shock or to a cloud complex situated within the local interstellar medium at $d < 60$ pc. The C IV to Si IV column density ratio in this gas is 8, a factor of 6 less than conductive interface models predict, but this discrepancy may be removed by considering the effects of self-photoionization within the cooling gas in the model calculations.

3. A broad ($b = 13$ km s^{-1}) and weak C IV absorption feature detected at $\langle v_{\rm helio} \rangle = -61$ km s^{-1} is not seen in other species. We tentatively ascribe this absorption to gas in a postshock region of an optically thin shock in the ζ Oph stellar wind.

Subject headings: H II regions — ISM: abundances — ISM: general — stars: individual (ζ Ophiuchi) — ultraviolet: stars

1. INTRODUCTION

The path to ζ Ophiuchi (HD 149757, HR 6175) has historically been one of the most studied interstellar sight lines in the sky. Because of its high effective temperature (31,900 K; Code et al. 1976) and moderate mass-loss rate ($\dot{M} = 6.3 \times 10^{-8}\ M_\odot$ yr^{-1}; see Howarth & Prinja 1989) in the form of a high-speed wind, ζ Oph offers an opportunity to study the interaction of a hot star and its immediate environment. The ionizing radiation from ζ Oph produces the H II region Sharpless 27, while the interaction of the wind with surrounding material likely creates the prominent bow shock evident in [O III] emission (Gull & Sofia 1979) and dust emission (Van Buren & McCray 1988). Spectroscopic studies of the sight line provide additional information about atoms and molecules associated with several diffuse cloud complexes that are well separated in velocity. Observations of highly ionized atoms along the sight line to ζ Oph therefore make it possible to study the presence or absence of these species at velocities associated with a variety of interstellar environments.

High-resolution Na I and Ca II observations (Hobbs 1969, 1973a; Marschall & Hobbs 1972) indicate that there are at least six distinct absorption components along the sight line, concentrated into general complexes centered near heliocentric velocities of −15 and −26 km s^{-1}. At least some of the −26 km s^{-1} absorption occurs within a diffuse cloud complex located near the Sun ($d < 60$ pc), whereas the −15 km s^{-1} absorption is primarily associated with diffuse clouds within about 20 pc of ζ Oph (Frisch 1981; Frisch & York 1984). Spectroscopic data from the *Copernicus and International Ultraviolet Explorer* (*IUE*) satellites provide extensive information about the physical conditions and distribution of the molecular and neutral gas in these two complexes (Morton 1975; Pwa & Pottasch 1986), and recent Goddard High-Resolution Spectrograph (GHRS) observations of heavy elements in the neutral gas reveal widely varying gas phase abundances between the two diffuse cloud complexes (Savage, Cardelli, & Sofia 1992).

Investigators probed for highly ionized gas toward ζ Oph using the spectrographs of the *Copernicus* and *IUE* observatories, but the data were of insufficient quality to study the detailed component structure of the absorption lines. To more fully explore the velocity distribution of the highly ionized gas along this line of sight, we have obtained GHRS spectra span-

[1] Based on observations obtained with the Goddard High-Resolution Spectrograph on the NASA/ESA *Hubble Space Telescope*, obtained at the Space Telescope Science Institute, which is operated by the Association of Universities for Research in Astronomy, Inc., under NASA contract NAS5-26555.

[2] Center for Space Research, Massachusetts Institute of Technology, Cambridge, MA 02139. Electronic mail: I:sembach@sundoggie.mit.edu.

[3] Washburn Observatory, Univerisity of Wisconsin, Madison, 475 North Charter Street, Madison, WI 53706.
Electronic mail: I:savage@madraf.astro.wisc.edu.

[4] Princeton University Observatory, Princeton, NJ 08544.
Electronic mail: I:ebj@astro.princeton.edu.

ning the UV resonance lines of Al III, Si IV, C IV, and N V. At the spectral resolution provided by this instrument, we can fully resolve the profiles and discern three principal components of the highly ionized gas absorption. A component associated with photoionized gas in the H II region surrounding ζ Oph was previously detected with the Copernicus and *IUE* satellites; the two remaining components have not previously been seen in the spectrum of ζ Oph and are probably associated with collisionally ionized gas.

The organization of this paper is as follows. In § 2 we present the GHRS observations of ζ Oph obtained for this study. We outline our analysis techniques in § 3. Section 4 contains a description of the general velocity structure of the ionized gas along the sight line. A discussion of the photoionized gas in the H II region surrounding ζ Oph is presented in § 5. In § 6 we analyze the principal broad Si IV and C IV absorption produced in collisionally ionized gas along the sight line and discuss possible sites where the absorption may be arising. In the Appendix we derive a new O VI column density limit for this gas based upon previous *Copernicus* observations. We use this O VI measurement to aid in interpreting the physical conditions in collisionally ionized gas along the sight line. Additional weak C IV absorption that is not seen in the other high ion lines is treated in § 7. A brief description of future prospects and concluding remarks are contained in § 8.

2. OBSERVATIONS

As part of the GHRS science verification (SV) program, high-resolution (FWHM ≈ 3.5 km s^{-1}) echelle-mode observations of the Al III, Si IV, C IV, and N V lines in the ultraviolet spectrum of ζ Oph were obtained. Light from ζ Oph entered the spectrograph through the small science aperture (SSA: 0.″25 × 0.″25), and exposures were obtained with digicon detector step pattern 6 with two spectrum samples per diode width. The exposures were acquired using four diode comb-addition and FP-split procedure #4 to reduce fixed-pattern noise introduced by the photon-counting digicon detectors. A background level was measured for each spectrum by obtaining full diode array interorder exposures as part of the detector scanning sequence and fitting a third-order polynomial to the resulting combined background. Details regarding the setup positions, detectors, gratings, and spectrograph can be found in the GHRS instrumentation handbook (Duncan & Ebbets 1990; Duncan 1992).

Intermediate-resolution (G160M) observations of the Si IV, C IV, and N V lines in the ζ Oph spectrum were also taken as part of the SV program. Poor centering of the starlight in both the large and small entrance apertures reduced the resulting signal-to-noise (S/N) ratios of the G160M data below expected values. The FP-split procedure was invoked only for the Si IV observations. The Si IV data have the full spectroscopic resolution (FWHM ~ 16 km s^{-1}) offered by the G160M grating and the SSA, whereas the C IV and N V data have degraded resolutions due to the *HST* spherical aberration in the large science aperture (LSA: 2.″0 × 2.″0). Table 1 contains the *HST* observation log identification, date of observation, wavelength coverage, and the interstellar species detected in each echelle and G160M observation.

We followed the data reduction procedure of Savage et al. (1992) for data extraction, spectrum merging, background processing and subtraction, and wavelength calibration of the data using software available at the Space Telescope Science Institute and the University of Wisconsin-Madison as of 1992 August. For the echelle data, we applied second-order scattered light corrections equal to 4% of the average net spectra according to the prescription outlined by Cardelli, Ebbets, & Savage (1990). The intermediate-resolution G160M intensity values did not require a scattered light background correction. The combined echelle data have S/N $\approx$ 30–60 and a heliocentric zero-velocity uncertainty of 3.5 km s^{-1} (1 σ). The combined intermediate-resolution Si IV, C IV, and N V data have S/N $\approx$ 140, 80 and 70, respectively.

In Figure 1 we show the Al III and high ionization profiles obtained with the GHRS echelle gratings over the heliocentric velocity range[5] from -160 km s^{-1} to $+160$ km s^{-1}. We illus-

[5] We adopt the heliocentric rest frame for all velocities in this paper; $v_{\rm LSR} = v_{\rm helio} + 13.9$ km s^{-1} for the ζ Oph sight line.

TABLE 1

GHRS OBSERVATIONS OF IONIZED GAS TOWARD ζ OPHIUCHI

Identification	Date (year/day)	Grating/[b] Order	Aperture[c]	$\lambda_{\rm min}$ (Å)	$\lambda_{\rm max}$ (Å)	Exposure Time[d] (s)	Species Observed
Z0LD021QM	1991/141	Ech-A/45	SSA	1234.8	1241.4	179.2	N V λ1238; Mg II λ1239
Z0LD0221M	1991/141	Ech-A/41	SSA	1388.5	1395.3	230.4	Si IV λ1393; 12CO
Z0LD0222M	1991/141	Ech-A/40	SSA	1388.3	1395.8	153.6	Si IV λ1393; 12CO, 13CO
Z0LD0223M	1919/141	Ech-A/40	SSA	1397.5	1404.8	153.6	Si IV λ1402
Z0LD0227M	1991/142	Ech-A/36	SSA	1545.9	1554.2	153.6	C IV λλ1548, 1550
Z0LD020TT	1991/141	Ech-B/30	SSA	1857.2	1867.2	76.8	Al III λ1862
Z0RZ0217T	1992/184	G160M	SSA	1374.2	1410.0	102.4	Si IV λλ1393, 1402; 12CO, 13CO
Z0HU011RT	1991/058	G160M	LSA	1222.6	1258.7	3.2	N V λλ1238, 1242; Mg II λλ1239, 1240
Z0HU0126T	1991/058	G160M	LSA	1522.4	1557.7	3.2	C IV λλ1548, 1550
Z0HU0127T	1991/058	G160M	LSA	1542.4	1577.6	3.2	C IV λλ1548, 1550

[a] *HST* data archive identification.

[b] Echelle-A and Echelle-B observations have a resolution (FWHM) of approximately 3.5 km s^{-1}. G160M SSA observations have a resolution (FWHM) of approximately 18 km s^{-1}. G160M LSA observations have a degraded resolution with a narrow core (FWHM $\sim$ 20 km s^{-1}; light percentage $\sim$40%) and broad wings (FWHM $\sim$ 85 km s^{-1}; light percentage $\sim$60%).

[c] LSA = large (2.″0 × 2.″0) science aperture. SSA = small (0.″25 × 0.″25) science aperture. Only SSA observations were obtained using the FP-split procedure to reduce fixed-pattern noise.

[d] On-spectrum exposure time.

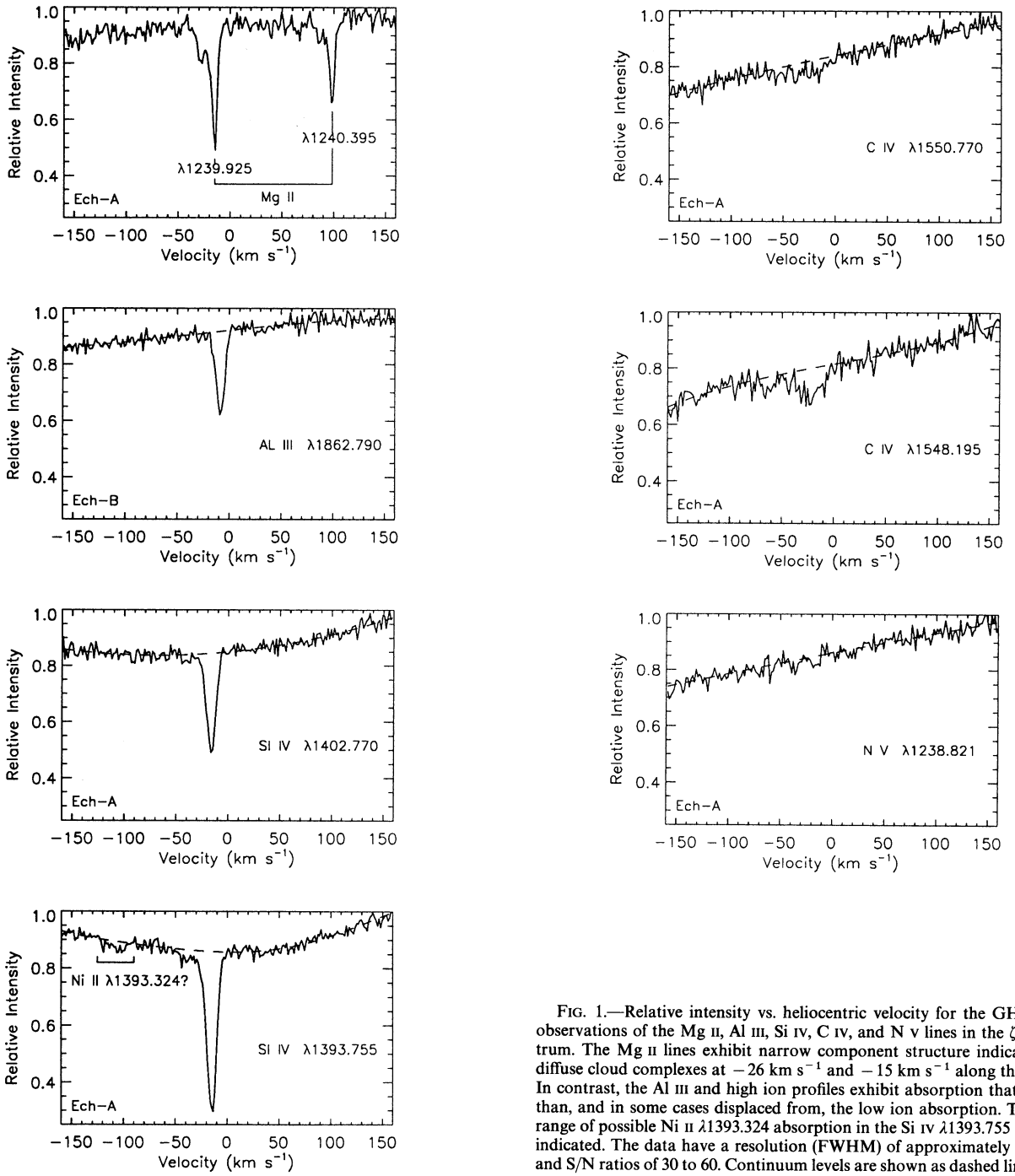

FIG. 1.—Relative intensity vs. heliocentric velocity for the GHRS echelle observations of the Mg II, Al III, Si IV, C IV, and N V lines in the ζ Oph spectrum. The Mg II lines exhibit narrow component structure indicative of the diffuse cloud complexes at -26 km s^{-1} and -15 km s^{-1} along the sight line. In contrast, the Al III and high ion profiles exhibit absorption that is broader than, and in some cases displaced from, the low ion absorption. The velocity range of possible Ni II λ1393.324 absorption in the Si IV λ1393.755 spectrum is indicated. The data have a resolution (FWHM) of approximately 3.5 km s^{-1} and S/N ratios of 30 to 60. Continuum levels are shown as dashed lines.

trate the high ion profiles obtained with the GHRS G160M grating in Figure 2. The dashed lines in the figures indicate the continua we adopt for our analysis of the data in later sections of the paper. The Mg II λλ1239.925, 1240.395 lines shown at the top of Figure 1 are present in the N V spectral region and are plotted for comparison with the high ionization lines. The Mg II lines exhibit a velocity structure similar to other low ionization lines (Savage et al. 1992), and they are clearly different from the high ion absorption structures. In particular, the distinct absorption systems located at -26 and -15 km s^{-1} in the Mg II profiles are much narrower than their approximate counterparts in the high ions. The weak absorption at $v \approx -108$ km s^{-1} present in both the echelle and G160M Si IV λ1393.755 observations is probably due to Ni II λ1393.324 ($f = 0.0222$, $W_\lambda < 3$ mÅ) absorption occurring in the two diffuse cloud complexes that show up in Mg II absorption. The G160M observations show structure in the high ionization profiles similar to that seen in the echelle observations, so we

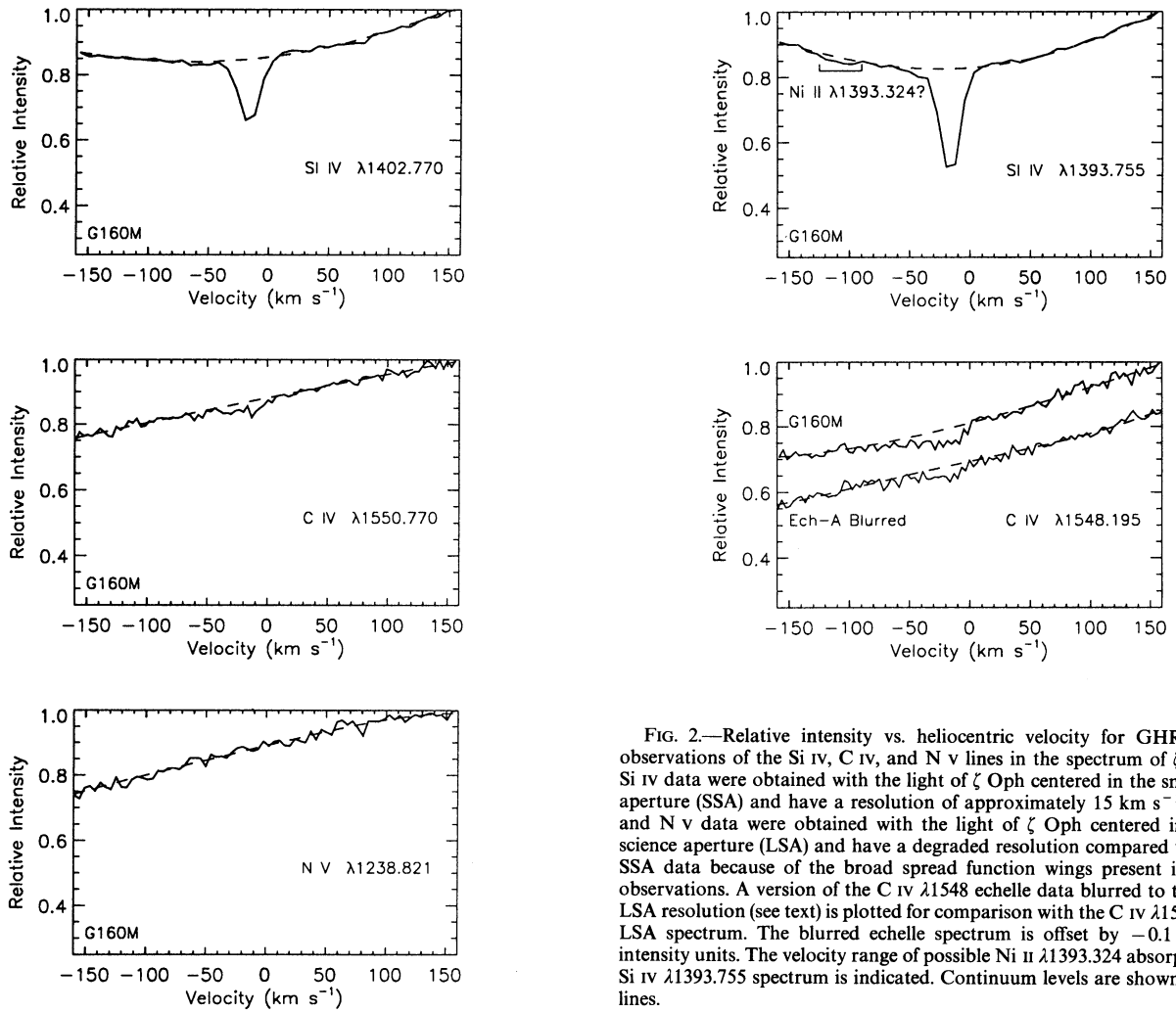

FIG. 2.—Relative intensity vs. heliocentric velocity for GHRS G160M observations of the Si IV, C IV, and N V lines in the spectrum of ζ Oph. The Si IV data were obtained with the light of ζ Oph centered in the small science aperture (SSA) and have a resolution of approximately 15 km s^{-1}. The C IV and N V data were obtained with the light of ζ Oph centered in the large science aperture (LSA) and have a degraded resolution compared to the Si IV SSA data because of the broad spread function wings present in the LSA observations. A version of the C IV λ1548 echelle data blurred to the G160M LSA resolution (see text) is plotted for comparison with the C IV λ1548 G160M LSA spectrum. The blurred echelle spectrum is offset by −0.1 in relative intensity units. The velocity range of possible Ni II λ1393.324 absorption in the Si IV λ1393.755 spectrum is indicated. Continuum levels are shown as dashed lines.

base our scientific interpretations primarily on the higher resolution echelle data and refer to the G160M data only when necessary.

3. ANALYSIS

3.1. *Equivalent Widths*

In Table 2 we list the equivalent widths for the highly ionized gas lines seen in the echelle spectra of ζ Oph. We adopted the equivalent width and error calculation procedures outlined by Sembach & Savage (1992). We fit a low-order (<5) Legendre polynomial to the data on both sides of each line to estimate the continuum. The listed errors account for continuum placement uncertainties and Poisson noise fluctuations within the line. We estimate that background removal for the echelle data is accurate to $\pm 1\%$ using the calibrations cited in § 2. A 1% uncertainty in the background level leads to an error of 0.2–0.4 mÅ for the equivalent widths listed in Table 2; this error is not included in the $\pm 1\ \sigma$ errors listed in the table. The value of S/N in the continuum interpolated to the line center is also listed in Table 2 for each line.

Independent equivalent width measurements of the ionized gas lines in the ζ Oph spectrum are compiled in Table 3. These equivalent widths are based upon measurements of the G160M observations shown in Figure 2 and previous estimates made by investigators using the *IUE* and *Copernicus* satellites. The two independent *IUE* equivalent width measurements (Pwa & Pottasch 1986 and our own measurements) are derived from combined high-dispersion (FWHM ≈ 20–25 km s^{-1}) *IUE* data. The GHRS echelle and G160M measurements yield similar results to the two sets of *IUE* measurements for the Al III λ1862, Si IV λλ1393 and 1402, and N V λ1238 lines. Equivalent widths of the Si IV λ1393 line and Al III λ1862 lines based upon *Copernicus* data (FWHM ≈ 12 km s^{-1}) (Morton 1975) differ significantly from the GHRS and *IUE* values, possibly because of improperly removed background levels in the *Copernicus* data.

The GHRS echelle observations of the C IV lines yield larger equivalent widths than those based on data obtained at lower resolution (see Table 3). We attribute the differences to systematic continuum placement uncertainties for broad weak lines in the lower resolution data. The C IV G160M LSA observations shown in Figure 2 have a substantially degraded resolution compared to the Si IV G160M SSA observations owing to the use of the large science aperture, which introduces broad (FWHM ~ 85 km s^{-1}) spread function wings into the spectra as a result of the *HST* spherical aberration. These wings contain about 60% of the light compared to 40% in the narrow (FWHM ~ 20 km s^{-1}) core. We calculated the appearance of

TABLE 2

EQUIVALENT WIDTHS AND INTEGRATED COLUMN DENSITIES[a]

Ion	λ (Å)	S/N[b]	$W_\lambda \pm 1\,\sigma$ (mÅ)	Integrated Column Density[c] $(-1\,\sigma)$	log N	$(+1\,\sigma)$	Integrated Range[d] v_-(km s^{-1})	v_+(km s^{-1})
Al III	1862.790	52	20.9 ± 1.1	12.42	12.44	12.46	−35	+5
Si IV	1393.755	58	40.1 ± 1.5	12.77	12.79	12.80	−50	+5
Si IV	1402.770	48	22.9 ± 1.4	12.76	12.79	12.81	−50	+5
C IV	1548.195	28	24.4 ± 3.1	12.74	12.80	12.86	−75	+5
C IV	1550.774	37	12.7 ± 2.3	12.73	12.81	12.88	−75	+5
N V	1238.821	41	3.0 ± 1.7	...	...	<12.48[e](2 σ)	−75	+5

[a] Equivalent width and column density results from GHRS echelle-mode data obtained at 3.5 km s^{-1} resolution. The lower resolution GHRS G160M results are listed in Table 3.

[b] Approximate S/N in the continuum at line center found by interpolation between regions adjacent to the line.

[c] Integrated column density and 1 σ error. Since the lines in this study are resolved, the column density is determined by direct integration of the $N(v)$ profile for each line.

[d] Velocity integration range used to determine the equivalent width and column density.

[e] For N V we report the 2 σ upper limit to the column density. The direct integration values for log N(N V) and ±1 σ limits to log N(N V) are 11.83, 12.17, and 12.36 dex.

the C IV λ1548 line at the degraded resolution and sampling interval of the C IV G160M data by convolving the echelle data with this LSA spread function. Equivalent width measurements of the C IV λ1548 line in this blurred echelle spectrum, shown under the G160M C IV λ1548 spectrum in Figure 2, resulted in a value $W_\lambda = 12$ mÅ, comparable to the G160M LSA measurement for the same line. Both the blurred echelle data and the G160M LSA data result in C IV λ1548 equivalent widths that are a factor of 2 smaller than the equivalent width measured for the fully resolved C IV echelle data acquired in the SSA. Continuum placement for lower resolution measurements of features this weak is clearly a major source of uncertainty.

3.2. *Column Densities*

In the limit where an absorption line is resolved, the column density per unit velocity of the absorption, $N(v)$ (atoms cm^{-2} [km s^{-1}]$^{-1}$), is described by

$$N(v) = \frac{(m_e c/\pi e^2)}{f\lambda}\,\tau(v) = 3.768 \times 10^{14}\,\frac{\tau(v)}{f\lambda}, \qquad (1)$$

where $\tau(v) = \ln[I_c(v)/I(v)]$ is the inferred optical depth of the line at velocity v, f is the oscillator strength of the transition, and λ is the wavelength in angstroms. The instrumental resolution of the echelle-mode observations (FWHM = 3.5 km s^{-1}) is smaller than the width of the lines if they arise in gas with $T \geq 10^4$ K; at $T = 10^4$ K the Doppler FWHM intensity would be 4.1, 4.1, 6.2, and 5.7 km s^{-1}, for Al III, Si IV, C IV, and N V, respectively. On average, H II regions have $T \approx 8000$ K (see Spitzer 1978), and the high resolution available with the GHRS echelle gratings insures that the Al III and Si IV lines are resolvable for $T > 7000$ K, whereas the C IV and N V lines are resolvable for $T > 3500$ K. Charge exchange reactions with

TABLE 3

ADDITIONAL EQUIVALENT WIDTH MEASUREMENTS[a]

Ion	λ (Å)	W_λ(G160M)[b] (mÅ)	W_λ(*IUE*)[c] (mÅ)	W_λ(*IUE*)[d] (mÅ)	W_λ(*Copernicus*)[e] (mÅ)
Al III	1854.716	...	41.4 ± 2.6	48.0 ± 9.0	57:
Al III	1862.790	...	22.5 ± 3.8	22.0 ± 9.0	34:
Si IV	1393.755	39.3 ± 0.9	35.7 ± 5.6	33.5 ± 6.3	24.7 ± 1.5
Si IV	1402.770	24.2 ± 1.1	16.9 ± 3.7	16.6 ± 6.5	17.9 ± 1.5
C IV	1548.195	14.9 ± 2.4[f]	10.6 ± 7.4	<8	<12
C IV	1550.774	7.8 ± 1.6[f]	9.2 ± 6.5	<5	...
N V	1238.821	1.1 ± 1.7	2.2 ± 6.2	<3	<3.8
N V	1242.804	...	<12	<3	<2.3

[a] Limits denoted by " < " are 2 σ upper limits. All other errors are 1 σ errors.

[b] GHRS G160M measurements by the authors.

[c] *IUE* measurements by the authors. Six well-exposed images from the *IUE* data archive (SWP 09689, 14428, 19043, 21166, 25461, 36122) were summed and used to construct a composite spectrum with S/N ≈ 25.

[d] *IUE* measurements and limits given by Pwa & Pottasch 1986.

[e] *Copernicus* measurements and limits given by Morton 1975. A colon indicates an uncertain value.

[f] The C IV G160M measurements were obtained with the light of ζ Oph in the LSA. The broad wings of the intrumental spread function may introduce systematic continuum placement errors not reflected in the listed ±1 σ values.

neutral hydrogen do not permit appreciable concentrations of highly ionized atoms to accumulate in cold, neutral gas clouds (Blint, Watson, & Christensen 1976; Christensen, Watson, & Blint 1977). The measured widths (FWHM) of the ionized gas lines are 9.5, 11.0, and 23.8 km s^{-1} for Al III, Si IV, and C IV, respectively. Therefore, we believe the observed profiles are fully resolved.

Direct integration of $N(v)$ over all velocities defining the line yields the total column density of the species, $N = \int N(v)dv$. We used the wavelengths and f-values listed in the atomic data compilation by Morton (1991) and obtained the column densities of Al III, Si IV, C IV, and N V listed in Table 2 by integrating equation (1) over the velocity intervals shown in the last two columns. The excellent agreement in the values of log N for the two members of the Si IV and C IV doublets is further proof that the profiles are fully resolved. For a discussion of the effects of unresolved saturated structure on the $N(v)$ profiles for doublet lines see Savage & Sembach (1991).

To calculate the column densities of lines as kinematically simple as those shown in Figure 1, one can also fit Gaussian optical depth components to the observed profiles. We specified each absorption component by a central velocity, $\langle v_i \rangle$; Doppler parameter, b_i [$=(2kT\ \mathrm{m}^{-1})^{1/2}$]; and column density, N_i. We adopted the profile fitting procedure outlined by Sembach, Danks, & Savage (1993) in calculating these quantities and their errors for the Al III, Si IV, and C IV lines. The results of the profile fits are compiled in Table 4. The finite GHRS instrumental resolution was incorporated into the χ^2 minimization by convolving the theoretical fit with a Gaussian instrumental spread function having FWHM = 3.5 km s^{-1}. For the Si IV and C IV data, we fit both members of each doublet simultaneously. In all cases, we fit two components to the profiles. Fitting two components instead of one improved the χ^2 statistics over the single component values by 25% for the C IV data, 40% for the Si IV data, and 8% for the Al III data. The small improvement in the χ^2 statistic for the double component fit to the Al III data attests to the inherent weakness of the second Al III feature. The total column densities derived by fitting the data with discrete components are nearly identical to those derived from direct integration of the $N(v)$ profiles. The errors listed in Table 4 account for uncertainties in $\langle v_i \rangle$, b_i, and N_i due to Poisson noise fluctuations, the dominant source of error in the computed values.

TABLE 4

PROFILE FIT RESULTS[a]

Ion	Lines Used	$\langle v_i \rangle$ (km s^{-1})	b_i (km s^{-1})	Log N_i
Al III	λ1862	-7.8 ± 0.2	4.3 ± 0.2	$12.38 \pm^{0.02}_{0.02}$
		-14.4 ± 0.7	3.2 ± 0.5	$11.56 \pm^{0.08}_{0.10}$
Si IV	λλ1393, 1402	-15.0 ± 0.2	5.3 ± 0.2	$12.74 \pm^{0.01}_{0.01}$
		-28.4 ± 6.6	15.8 ± 4.4	$11.82 \pm^{0.12}_{0.16}$
C IV	λλ1548, 1550	-23.7 ± 5.0	18.5 ± 4.8	$12.73 \pm^{0.11}_{0.14}$
		-61.0 ± 9.4[b]	12.8 ± 8.0	$12.19 \pm^{0.23}_{0.54}$

[a] The results of profile fitting to the GHRS high ion echelle-mode observations are listed along with their $\pm 1\ \sigma$ errors. The various quantities are central velocity of the component, $\langle v_i \rangle$; Doppler spread velocity of the component, b_i; and logarithmic column density of the component, log N_i. The profile fits are illustrated in Fig. 3.

[b] The measured 2 σ upper limits for other species at this velocity from direct integration of the observed profiles are log N(N I) < 11.8, log N(Fe II) < 10.8, log N(Al III) < 11.3, log N(Si IV) < 11.3, and log N(N V) < 12.1.

4. VELOCITY STRUCTURE OF THE IONIZED GAS OBSERVED BY GHRS

Low ionization lines of dominant ions such as O I, N I, Mg II, Cr II, Mn II, Fe II, and Ni II toward ζ Oph have been studied in detail at 3.5 km s^{-1} resolution with the GHRS (Savage et al. 1992). The low ion lines show two general groupings of components near −26 and −15 km s^{-1}. Each grouping consists of blends of components that are more clearly separated in the 0.5 km s^{-1} resolution Na I data obtained by Hobbs (1969). The Na I data shows components near −26.7, −25.5, −17.5, −14.4, −12.6, and −10.0 km s^{-1}. The velocity distributions of the low and high ionization lines differ dramatically, as one can see by comparing the Mg II and high ion profiles in Figure 1 (see also the low ion lines illustrated by Savage et al. 1992).

We display the results of our component fitting analysis of the previous section in Figure 3, where we have plotted the data as plus signs and the fit results as solid lines. Dashed lines in the figure indicate continuum levels. We find the following velocity structure for the ionized gas toward ζ Oph as seen in our high-resolution GHRS data.

1. Al III.—The Al III λ1862 profile shows narrow, but overlapping, structures located at -14.4 ± 0.7 km s^{-1} ($b = 3.2 \pm 0.5$ km s^{-1}, log $N = 11.56 \pm^{0.08}_{0.10}$) and -7.8 ± 0.2 km s^{-1} ($b = 4.3 \pm 0.2$ km s^{-1}, log $N = 12.83 \pm^{0.02}_{0.02}$). We find no evidence for Al III absorption associated with the −26 km s^{-1} diffuse cloud complex seen in neutral species (see Savage et al. 1992) or with the broad weak component near −26 km s^{-1} seen in Si IV and C IV.

2. Si IV.—The Si IV profiles exhibit a strong narrow component ($b = 5.3 \pm 0.2$ km s^{-1}, log $N = 12.74 \pm^{0.01}_{0.01}$) centered at -15.0 ± 0.2 km s^{-1} and a partly overlapping, broad, shallow component ($b = 15.8 \pm 4.4$ km s^{-1}, log $N = 11.82 \pm^{0.12}_{0.16}$) centered at -28.4 ± 6.6 km s^{-1}. The two components are easily visible in both the echelle observations and the high S/N (~100) G160M SSA observations shown in Figures 1 and 2.

3. C IV.—The C IV profiles reveal two broad, weak absorption components, one centered at -23.7 ± 5.0 km s^{-1} ($b = 18.5 \pm 4.8$ km s^{-1}, log $N = 12.73 \pm^{0.11}_{0.14}$) and another centered at -61.0 ± 9.4 km s^{-1} ($b = 12.8 \pm 8.0$ km s^{-1}, log $N = 12.19 \pm^{0.23}_{0.54}$). The −61 km s^{-1} component is unique to the C IV data. It is detected at a 3 σ level with $W_\lambda(1548) = 4.8 \pm 1.6$ mÅ from direct integration of the profile between −75 km s^{-1} and −45 km s^{-1}. This detection level is consistent with the profile fitting result. For the other ionized species, the 2 σ upper limits for detections of the −61 km s^{-1} component between −75 km s^{-1} and −45 km s^{-1} are log N(Al III) < 11.3, log N(Si IV) < 11.3, and log N(N V) < 12.1.

4. N V.—We were unable to fit a profile to the N V λ1238 line data. From direct integration of the λ1238 line between −75 and +5 km s^{-1}, we set a 2 σ column density limit of log N (N V) < 12.48 [$W_\lambda(1238) < 6.4$ mÅ]. The GHRS intermediate-resolution observations are not of sufficient quality to make a definitive N V detection either, but we can place a 2 σ equivalent width of 4.5 mÅ on the λ1238 line in the G160M LSA spectra (Table 3). Combining the independent echelle and G160M results, we derive a combined 2 σ column density limit of log N(N V) < 12.32 [$W_\lambda(1238) < 4.4$ mÅ].

A 7.2 km s^{-1} velocity difference separates the strongest absorption component in the Al III ($\langle v \rangle = -7.8$ km s^{-1}) and Si IV ($\langle v \rangle = -15$ km s^{-1}) lines. The Al III absorption has a weak component at −14.4 km s^{-1} near the peak of the Si IV

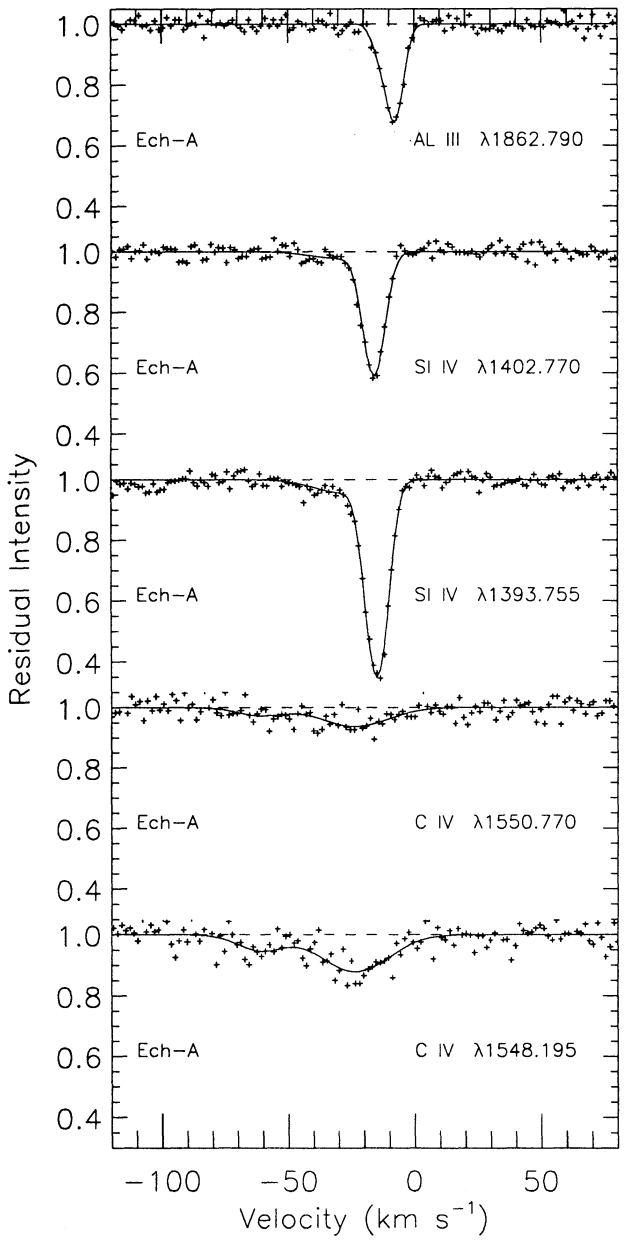

FIG. 3.—Residual intensity *vs.* heliocentric velocity for the Al III, Si IV, and C IV echelle data shown in Fig. 1. The data points are plotted as plus signs. The absorption profiles derived from the component fitting analysis discussed in § 3.2 are shown as solid lines. A summary of the profile fit results and component structure of the lines is given in Table 4. Continuum levels are indicated by dashed lines.

absorption. Using the most current wavelength calibrations available as part of the standard GHRS echelle data processing software, we expect that the quoted velocities of the lines are accurate to ± 3.5 km s^{-1} (1 σ), a factor of 2 smaller than the observed separation.

To confirm that the difference between the main Al III and Si IV absorption components is not due to GHRS wavelength calibration problems, we obtained six well-exposed images from the *IUE* data archives to check for systematic shift between the GHRS and *IUE* data for these two species. Using the *IUE* data reduction procedures described by Sembach & Savage (1992), we constructed an *IUE* spectrum of ζ Oph with S/N = 20–30. We measured the centroids of the Si IV λ1393 and Al III λ1862 lines and found a central velocity difference of 8 km s^{-1}, very similar to the offset we find for the GHRS data (see also Pwa & Pottasch 1986).

Given the modest resolution at which the Al III and Si IV lines have always been observed, we also investigated whether a systematic shift in the laboratory rest wavelength of the Al III or Si IV lines could account for the observed velocity disparity between the two species. Isberg (1968) quotes a measured laboratory wavelength of 1862.7895 $\pm$ 0.0035 Å for the Al III line, which translates into a velocity uncertainty of 0.6 km s^{-1}. Martin & Zalubas (1983) quote a wavelength of 1393.7546 $\pm$ 0.0059 for the Si IV line, which corresponds to a velocity uncertainty of 1.3 km s^{-1}. Adding these velocity errors in quadrature results in a total error of only 1.4 km s^{-1}, a factor of 5 smaller than the observed 7.2 km s^{-1} difference between the Si IV and Al III central velocities. There is no duplication of the apparent velocity offset in GHRS observations of interstellar Al III and Si IV profiles in the spectrum of ξ Per (Cardelli et al. 1991; Savage et al. 1991. Federman et al. (1993) have recently detected P III absorption at a heliocentric velocity of -8 km s^{-1}. P III has a very similar creation and destruction ionization potentials (19.7 eV and 30.2 eV) to those of Al III (18.8 eV and 28.4 eV) and is sensitive tracer of undepleted gas in H II regions. This finding gives some assurance that the modest velocity difference between the peak absorption in the Al III and Si IV lines for the ζ Oph sight line is not an artifact of the data reduction process or the assigned rest wavelengths but, rather, is due to the physical processes governing the absorption produced by these two species along the sight line.

It is unlikely that photospheric absorption is responsible for the high ion absorption structure discussed above. ζ Oph has a projected rotational velocity of 350 km s^{-1} (Slettebak 1966; Conti & Ebbets 1977) and a heliocentric radial velocity of -19 km s^{-1} (Blaauw 1961; Morton 1976). Photospheric features in the spectrum of ζ Oph are about 5 times broader than the weak -26 km s^{-1} Si IV and C IV components or the -61 km s^{-1} C IV component. The very large breadth of the photospheric lines reduces continuum level ambiguities and makes fitting the stellar continuum simpler. Also, the observed C IV absorption occurs against a well-developed P Cygni profile that spreads the stellar absorption over many hundreds of kilometers per second.

The rapid rotation of ζ Oph introduces high-order nonradial pulsations which produce transient changes in the shapes of the He I λ6678 emission line and nearby continuum (Vogt & Penrod 1983; Kambe, Ando, & Hirata 1990; see also Walker, Yang, & Fahlman 1979). Distortions seen in the He I emission profile often have widths comparable to the widths of the observed Si IV and C IV absorption at -26 km s^{-1}. The distortions are short-lived (hours) and traverse the He I profile quickly. It is unlikely that the observed -26 km s^{-1} feature is a product of these oscillations since its shape is so similar in the Si IV small-aperture echelle and intermediate-resolution data taken more than a year apart. Unfortunately, we do not have useful information about possible time variations in the C IV absorption near -26 and -61 km s^{-1}. The repeat integrations were obtained with the G160M mode and the LSA (see Table 1), and the broad wings on the instrumental spread function due to the *HST* spherical aberration makes it difficult to reliably study such weak features (see § 3.1).

5. THE ζ OPHIUCHI H II REGION

5.1. *General Properties*

Reynolds (1988) estimated an angular radius of 9°.2 for the H II region surrounding ζ Oph based upon Hα photographs in the literature. At a distance of 140 pc, this angular size corresponds to a radius of about 11 pc, somewhat smaller than the Strömgren radius of 15 pc found by Reynolds & Ogden (1982). Measurements of the Hα, [N II] λ6584, and [S II] λ6716 lines arising in the H II region indicate that $n_e \approx 4$ cm^{-3} and $T \approx 7000$ K (Reynolds & Ogden 1982; Reynolds 1988). These same studies indicate that the Hα emission arising in the H II region is described well by a single Gaussian component centered on a heliocentric velocity of -13 ± 1 km s^{-1}, which is in accord with the less precise value of -8 ± 5 km s^{-1} quoted by Georgelin & Georgelin (1970). The Hα emission is broad, $b = 13.4 \pm 0.2$ km s^{-1}, but the central Hα velocities found by Reynolds & Ogden (1982) for locations within 2° of the star differ by no more than 3 km s^{-1}.

The similarity between the velocities of the ζ Oph H II region and the diffuse H I cloud grouping near -15 km s^{-1} may be the result of proximity but does not necessarily imply physical interaction. Hollenbach, Chu, & McCray (1976) showed that significant amounts of molecular gas (in particular, H_2) can be produced in thin sheets swept up by expanding bubbles around early-type stars. A two-component model incorporating a cold, dense ($T = 25$ K, $n = 2000$ cm^{-3}) cloud and cool, diffuse ($T = 110$ K, $n = 500$ cm^{-3}) cloud near the star reproduce the molecular observations well (Black & Dalgarno 1977; see also Joshi & Tarafdar 1975; Jura 1975; Wright & Morton 1979), although de Boer & Morton (1979) noted that the C I line strengths indicate that the outer region may have much lower densities ($n \leq 30$ cm^{-3}).

Wright & Morton (1979) studied the populations of the rotational and vibrational levels of the HD molecule in the -15 km s^{-1} complex and concluded that it is located approximately 28 pc from the star, beyond the edge of the H II region defined by the observable Hα emission. Crutcher (1977) calculated a distance of 25 pc based upon a study of the carbon recombination lines arising within the cloud. If these distance estimates are correct, it is unlikely that the cloud complex is physically associated with the ionized gas in the H II region. Perhaps the similarity of the velocities of these two regions is indicative of a larger region of gas in which both the ζ Oph environment and surrounding clouds are embedded. The CO emission line study of Liszt (1992) strongly suggests that the dense neutral material occulting ζ Oph occurs in a coherent structure centered near the star. Both views may be correct since Frisch & York (1984) have determined from Na I absorption line observations of three stars within several degrees of ζ Oph that some portion of the main interstellar complex at -15 km s^{-1} lies within about 60 pc of the Sun (see their spectra for HD 149662 and HD 149807, stars of spectral type F2 V at distances of only 55 and 87 pc, respectively).

High-resolution observations of the excited levels of molecular lines toward ζ Oph show multiple components within the -15 km s^{-1} grouping, and in some cases the molecular lines (e.g., OH and CH^+) are shifted by a few kilometers per second relative to the atomic absorptions (Hobbs 1973b; Crutcher 1979). These velocity shifts have been attributed to shocks near the -15 km s^{-1} complex (Elitzur & Watson 1978a, 1978b, 1980; Draine 1986), although the inclusion of H_2 photodissociation by the background ultraviolet field may complicate the interpretation (Monteiro et al. 1988) While the modest shock speeds ($v_{shock} \sim 10$ km s^{-1}) required to explain the shifts do not produce signficant amounts of highly ionized gas and cannot be responsible for the velocity similarities between the narrow Si IV component and the neutral gas absorption, we cannot exclude the possibility that a fraction of the high ion absorption near -15 km s^{-1} may occur in a more diffuse medium surrounding the complex, perhaps at the photoionized boundaries of one or more clouds.

It is not clear how the bow shock structure evident in [O III] emission (Gull & Sofia 1979) and dust emission (Van Buren & McCray 1988) relates to the diffuse cloud structures just discussed. The bow shock is probably confined to within a few parsecs of ζ Oph (see § 6.3). Measures of the [O III] velocities associated with the bow shock gas will be of crucial importance for establishing whether there is a connection between bow shock and the observed Si IV absorption near -15 km s^{-1}.

5.2. *Photoionized* Si IV

The most striking aspect of the Si IV and C IV profiles shown in Figures 1–3 is the presence of a strong, narrow Si IV component that has no counterpart in the C IV lines. If the ionization were established by electron collisions in thermal equilibrium, we would expect appreciable concentrations of Si IV only at T near 10^5 K (Shull & Van Steenberg 1982). Clearly, the gas that produces the narrow Si IV component must be cooler than this temperature, since the line width is consistent with a Doppler thermal broadening of only 5×10^4 K. In steady state at this temperature, the fraction of triply ionized silicon should be two orders of magnitude lower than the peak fraction at 10^5 K.

At a temperature near 10^5 K, a gas with a cosmic composition cools by radiation more rapidly than it recombines. As a result, appreciable concentrations of highly ionized species may be expected at temperatures well below those where equilibrium concentrations have their peak values (Kafatos 1973). Calculations by Shapiro & Moore (1976) for gas that is undergoing isochoric cooling show that even at 10^4 K as much as 10% of the carbon and silicon atoms may be found in the triply ionized state. This picture is inconsistent with our data, since there should be about 20 times as much C IV as Si IV if cosmic abundances apply. If the elements are depleted from the gas phase, the discrepancy would be even worse, since silicon is generally found to be more depleted than carbon (e.g., compare the results of Barker et al. 1984 and Van Steenberg & Shull 1988 for silicon with those of Cardelli et al. 1993 for carbon).

We propose that the narrow component of Si IV is produced by photoionization within the H II region surrounding ζ Oph. Morton (1975) arrived at a similar conclusion based upon the velocity correspondence between the absorption lines of Si IV and other ionized gas species such as N II, N II**, Si II*, Si III, S III, and Fe III observed with the *Copernicus* satellite. Of these ions, those in excited fine-structure levels, such as N II** and Si II*, are particularly good tracers of H II region gas (Spitzer & Jenkins 1975) and have central velocities within 3 km s^{-1} of the Si IV central velocity.[6] Al III is also a good tracer of pho-

[6] All of the listed species were observed with the *Copernicus* U1 detector, which covers the wavelength range from 980 to 1420 Å in second-order diffraction. Morton (1975) made no attempt to reconcile the wavelength scale of this configuration with measurements using the other detector (V1) or other orders. For that reason, we cannot use his reported wavelengths to compare the velocities of these species directly with his measurement of Al III at 1862 Å.

toionized gas, and we detect an Al III component within 1 km s^{-1} of the Si IV component (see § 4). The radiative recombination coefficients for C IV and Si IV going to lower ionizations stages are roughly equal, and for both ions dielectronic recombinations are unimportant at $T = 7000$ K (Aldrovandi & Pequignot 1973). Therefore, an energy distribution of ionizing photons that has a significant drop in flux between the third ionization potentials of silicon and carbon (33 and 48 eV, respectively) is the easiest way to explain the relative absence of a narrow component of C IV associated with this photoionized gas.

We can estimate the amount of line broadening due to turbulence in the Si IV region by adopting the temperature of $T = 7000$ K for the region (see § 5.1; this temperature is also plausible on theoretical grounds—see Spitzer 1978, § 6.1). From the measured profile width, $b = 5.3 \pm 0.2$ km s^{-1}, we infer a turbulent velocity, $4.7 < b_t < 5.1$ km s^{-1}, somewhat smaller than the $b_t = 6.6$ km s^{-1} rms value found by Reynolds & Ogden (1982) in their analysis of the Hα and [N II] emission toward ζ Oph. The larger values of b_t derived from the emission line studies may be due to a finite beam size (50′ in diameter) compared to the infinitesimal solid angle of the absorption line data or to differences in the distribution of the Si IV and lower ionization species in the H II region.

5.3. *High Ion Abundances: Observations versus Theory*

By measuring the angular diameter and flux distribution of ζ Oph, Code et al. (1976) found an effective temperature, $T_{\rm eff} = 31{,}910 \pm 2040$ K. Cowie, Taylor, & York (1981) estimated Si IV and C IV column densities in an H II region having an electron density $n_e = 1.0$ cm^{-3} and central star with $T_{\rm eff} = 30{,}000$ K using simple analytical expressions and the LTE stellar atmosphere models given by Kurucz (1979). They found $N(\text{Si IV}) = 7.8 \times 10^{13}$ and $N(\text{C IV}) = 5.7 \times 10^{12}$ cm^{-2}. The results are similar to those obtained by Black et al. (1980) for an ionization bounded nebula with a constant electron temperature of $T_e = 10^4$ K, but they are several times smaller than the non-LTE results of de Kool & de Jong (1985). For the simplistic model of the ζ Oph H II region having a uniform electron density of 4 cm^{-3} throughout, the column density estimates double to $N(\text{Si IV}) = 1.6 \times 10^{14}$ and $N(\text{C IV}) = 1.1 \times 10^{13}$ cm^{-2} since the predicted column densities scale as $n_e^{1/2}$. The model Si IV column density is about a factor of 30 larger than the observed value of 5.5×10^{12} cm^{-2}, while the predicted C IV column density is a factor of 10 larger than the upper limit of 1.2×10^{12} cm^{-2} obtained by fitting a component with the same width as the observed Si IV component ($b = 5.3$ km s^{-1}) to the observed C IV profiles at -15 km s^{-1}. The amount of C IV actually associated with the H II region may be considerably less because much of the absorption near -15 km s^{-1} is probably contributed by the broad C IV absorption discussed in § 6. Although not explicitly calculated, the amount of N V produced in an H II region around normal Population I O or B stars is very small because N V production requires 77 eV and hot star models have a strong He II absorption edge at 54 eV (see, for example, the ionization calculations by Dupree & Raymond 1983 for the column densities of highly ionized gas around helium-rich white dwarf stars).

Several competing effects may be responsible for the differences between the observed and predicted amounts of Si IV and C IV in the H II region. To reconcile the predicted and observed column densities by adjusting only the density in the inner portions of the H II region where the high ions are found requires $n_e \approx 5 \times 10^{-3}$ cm^{-3} in these locations, in contrast to the average value of $n_e \approx 4$ cm^{-3} found by Reynolds (1988). The size of the Strömgren sphere containing a species scales as $n_e^{-1/2}$; thus, the Si IV region with $n_e = 5 \times 10^{-3}$ cm^{-3} would be approximately 7 pc in radius, whereas the C IV region would be less than 1 pc in size (see Cowie, Taylor, & York 1981). The size of the corresponding ionized hydrogen sphere would exceed the limits of the observed Hα emission. It is unlikely that the differences between the observed and predicted values can be attributed to density variations alone in a classical spherical H II region.

Castor, McCray, & Weaver (1975) have proposed a multizone structure for circumstellar environments around hot stars. The circumstellar structure consists of an interior zone vacated by material ejected from the star mixed with some swept-up gas and a higher density shell containing an ionization gradient between H II and H I region species abutting the ambient interstellar gas. In such a model, photons from the star freely intercept the shell, since the interior zone has a very low density. The most highly ionized gas in the H II shell occurs at the largest velocities relative to the star. As the shell slows down and its optical depth increases, less ionized species are formed at lower velocities relative to the star. Since Al II and Si III have considerably different ionization potentials (18.8 vs. 33.5 eV, respectively), the velocity and ionization gradients across the shell may explain the 7 km s^{-1} difference seen in the peak of the Al III and Si IV absorption. Ionized gas flowing back into the vacated zone from the H II region shell may complicate this simple picture. There is also likely to be ionized gas associated with dense nonionized clouds remaining in the vacated region which, when subjected to the surrounding hot gas, evaporate and release material into the surrounding region (Osterbrock 1989, pp. 171–201).

Another reason for believing a simple, spherically symmetric shell model of the ζ Oph sight line may not be strictly applicable is that ζ Oph is a runaway star with an origin in the Sco-Cen association (Blaauw 1961; Berkhuijsen, Haslam, & Salter 1971; Beckenstein & Bowers 1974). Models of bow shocks around hot stars (Van Buren et al. 1990; MacLow et al. 1991) predict an ionization structure with a shocked, cooling gas layer between the H II region and the free flowing wind zone. Since ζ Oph has a bow shock seen in [O III] emission (Gull & Sofia 1979), interferometric observations of this ion could prove extremely valuable in deciding whether the observed narrow Al III and Si IV components are associated with the bow shock or whether they arise completely within the general H II region around the star.

When comparing predicted and observed Si IV and C IV column densities, one must consider that the EUV energy distributions for stars are generally poorly determined. Physical mechanisms that lead to an underestimation of short-wavelength opacities result in a harder photon energy distribution, which in turn leads to an overestimation in the predicted column densities of the highly ionized species. A stellar wind is capable of processing (and reprocessing) the photons required to create the high ions as well as restructuring the environment in the vicinity of the star. ζ Oph has a stellar wind with a C IV terminal velocity of approximately -1400 km s^{-1} and a mass-loss rate of 6.3×10^{-8} $M_\odot$ yr^{-1} (Snow & Morton 1976; Howarth & Prinja 1989). The presence of He I in the wind near the star may destroy photons from 24.6 to 54.4 eV as it is converted to He II, leaving fewer photons to create species such

as O III, Si IV, and C IV. Lucy (1983) noted that kinematically induced backscattering in chaotic wind regions can reduce the predicted line emission below that expected for smooth wind flow. Lucy also found that photon trapping by scattering complexes within a monotonic wind flow can destroy photons. These mechanisms are not included in the model flux values used to derive the predicted column densities discussed above. They result in lower predicted high ion column densities and are probably responsible for some of the differences between the predicted and observed values.

5.4. *The Effects of Dust on the High Ion* H II *Region Abundances*

In the previous discussions we have ignored the effects of dust on the structure and ionization of the H II region. The abundances of high ionization species such as Si IV and C IV are affected by the presence of dust in several ways. By absorbing photons having energies in the 30–50 eV range, the dust grains remove photons capable of ionizing species such as He I, C III, O II, and Si III. By absorbing photons at energies below 30 eV, the decreased abundances in the next lower ionization stage results in decreased production of the high ions. Sarazin (1977) showed that the [O II] intensity in an H II region around a single ionizing star with $T_{\rm eff} = 30{,}000$ K is reduced by a factor of 2 to 3 for a simple power-law dust attenuation at an optical depth of unity. CO, H I, and *IRAS* emission measurements (de Gues & Burton 1991) indicate that a hot, dusty region may exist near ζ Oph in which CO dissociation has occurred but grain destruction is not complete.

The optical depth of the dust in an H II region with heavy element abundance Z (relative to solar heavy element abundance $Z_\odot$) at a frequency ν is given by

$$\tau_\nu = \kappa_1 \left(\frac{\nu}{\nu_1}\right)^{\alpha} \left(\frac{Z}{Z_\odot}\right) R_\nu n_e f^{1/2} , \qquad (2)$$

where κ_1 is the dust opacity per atom of gas at $\nu = 1$ ryd, R_ν is the size of the region containing photons of frequency ν, n_e is the electron density, f, is the volume filling factor of the gas, and the values of κ_1 and α are constrained to $0.8 \times 10^{-21} \leq \kappa_1 \leq 2.5 \times 10^{-21}$ and $3 \geq \alpha \geq 1$ (see Sarazin 1976). To determine a lower limit to the distance a photon must travel before the dust optical depth reaches unity, we invert equation (2) and solve for R_ν with $f = 1$. The ionization potentials of Si III and C III are 33.5 eV and 47.9 eV, respectively. For a nebula with solar abundances ($Z = Z_\odot$), we find R_ν(Si IV) $> (27/n_e)$ pc and R_ν(C IV) $> (9/n_e)$ pc. A patchy dust distribution ($f < 1$; a typical value is $f = 0.04$; see Sarazin 1976) or subsolar abundances ($Z < Z_\odot$) results in larger values of R_ν(Si IV) and R_ν(C IV). The radii of the ionized spheres containing Si IV and C IV in an H II region with $n_e = 4$ cm^{-3} surrounding a $T_{\rm eff} = 30{,}000$ K star are R(Si IV) = 0.25 pc and R(C IV) = 0.002 pc (see Cowie et al. 1981). The H II region abundances of these ions should be unaffected by photon absorption due to dust, since the lengths required to reach a dust optical depth of unity are much larger the sizes of the Si IV and C IV bearing regions in front of ζ Oph, even for large values of n_e.

The theoretical column density estimates assume that the H II region gas has a solar composition. Subsolar abundances result when elements in the gas phase become locked into dust grains. To assign the differences between the observed and the larger predicted column densities solely to elemental depletions onto dust grains requires that carbon and silicon be depleted in the gas phase below their solar abundances by factors of 10 and 30, respectively. For a gas having $n(\mathrm{H_{tot}}) \approx 3$ atoms cm^{-3}, the typical depletions of carbon and silicon are approximately factors of 3 and 40 below their solar values (Jenkins 1987). GHRS measurements of the very weak C II] λ2324 line (Cardelli et al. 1993) have revealed that the abundance of carbon in the diffuse clouds near ζ Oph is a factor of 3 below solar. These depletions are similar to those needed to explain the differences in the observed and predicted column densities. Perhaps only a small fraction of the silicon and carbon locked into the grains has recently been liberated from the denser material near ζ Oph. Possible liberating mechanisms include shocks like the bow shock seen by Van Buren & McCray (1988) or grain sputtering by helium atoms in the expanding H II region (Aannstad 1973). With such liberation, enhancements of refractory elements (e.g. aluminum, calcium, titanium, chromium, iron) over their dense cloud depletions would likely be occurring within the H II region surrounding ζ Oph, since the return of refractories to the gas phase occurs much more easily than for carbon. Refractory element gas phase enhancements are not seen in the diffuse cloud near -15 km s^{-1} (Savage et al. 1992), although the similarity in velocity between the H II region gas and the diffuse clouds confuses the issue.

6. COLLISIONALLY IONIZED GAS

6.1. *General Considerations*

We turn now to the much broader, weak absorption features seen in Si IV and C IV centered at velocities of approximately -26 and -61 km s^{-1} (see Table 4). In contrast to the components discussed in the previous section, these features show virtually no accompanying Al III and have C IV column densities that greatly exceed their counterparts in Si IV. These relative abundances, along with the large line widths, are more consistent with the ionization being produced by electron collisions in high-temperature plasmas. The line widths are, however, about twice as broad as those for the expected thermal Doppler broadening of these ions at a temperature (10^5 K) that favors their production in collisional equilibrium. One can surmise that either there are multiple, narrower components that are blended to produce a broad feature or that large scale gas motions within a single region are responsible for the broadening. Still another possibility is that the temperature could indeed be as high as the value 4×10^5 K needed to broaden the lines to the observed widths. In equilibrium, the predicted abundances would be at least two orders of magnitude below the peak values (Shull & Van Steenberg 1982), but if the gas has been heated in a time that is short compared with the ionization time, the transfer to higher ionization stages may not yet be complete. This latter possibility fits in well with a proposed interpretation given below (in § 6.2).

The most plausible initial source of heating to reach 10^5 K (or greater) is from the passage of one or more shocks having a minimum velocity of 85 km s^{-1} (McCray & Snow 1979), coming either from randomly located, distant supernova explosions (Cox & Smith 1974; McKee & Ostriker 1977; Smith 1977) or from the collision of a fast, stellar wind with the ambient material (Castor et al. 1975; Weaver et al. 1977). When UV absorption lines from highly ionized species are observed, it is usually true that the velocity widths and centroid offsets are substantially lower than the velocity of a shock that was needed to create the ions (Jenkins 1978b). This condi-

tion applies to our features of Si IV and C IV centered near -26 km s^{-1} and leads to the conclusion (Cowie & Songaila 1986; Spitzer 1990) that we are probably viewing a secondary phenomenon, such as a conduction front between a reservoir of very hot gas and some adjacent, very much cooler material. Here, the hot gas that is detected in absorption is kinematically coupled to low-velocity gas by virtue of its being within an established zone of conduction and evaporation (or condensation) between the hot and cold phases (Cowie & McKee 1977; McKee & Cowie 1977). Some support for this picture in a general context has been provided by Cowie et al. (1979), who found a loose statistical association between the velocities of O VI profiles and those produced by atoms in lower stages of ionization. The primary hot gas, i.e., that which was subjected to the original shock and not subsequently influenced by interactions with cool gas, is probably not easily seen in UV absorption features because the turbulent velocity dispersion is too large (McKee & Ostriker 1977; Jenkins 1978b).

6.2. *Conductive Interfaces*

Borkowski, Balbus, & Fristrom (1990) gave a comprehensive description of the expected column densities, velocity dispersions (expressed in terms of average temperatures), and systematic velocity shifts for various ions that could be observed in planar, thermal conduction fronts at various stages of development. If we study these results, it is immediately apparent that the relative lack of N V (see Table 2) and O VI (see Appendix) in the line of sight to ζ Oph focuses our attention on the possiblity of a front in an early stage of development. Here, the dominant process is evaporation of the cold gas that occurs long before radiative cooling can establish a stable zone of hot gas that has had a chance to build an appreciable concentration of the most highly ionized species. For the interstellar pressure $p/k = 3.75 \times 10^3$ cm^{-3} K chosen by Borkowski et al., the age of the front is less than about 10^5 yr (the time scales inversely with pressure).

Our preferred value for the column density of C IV absorbing near -24 km s^{-1} ($\log N = 12.73$) agrees well with a plausible configuration for a young conduction front. At early times the source of hot gas is conductively heated, cool cloud material that should still have dust grains, rather than surrounding hot gas with presumably no heavy element depletions that is cooling and collapsing onto the interface.

Our measured Doppler parameter for Si IV absorbing near -28 km s^{-1}, $b = 15.8 \pm 4.4$ km s^{-1}, lends further support to the viewpoint that the interface is young. Theoretical mean ionic temperatures for an age less than 10^5 yr correspond well to our observed Si IV profile widths, while older fronts should show a profile that is near our $-2\,\sigma$ limit for b. The observed values of b for C IV span the entire range of theoretical values and thus are inconclusive on this test. In regions that contain most of the C IV and Si IV, systematic flow velocities are less than 2 km s^{-1}, in agreement with our data that show no significant differences in the velocity centroids of these two species.

One glaring discrepancy between our findings and the model of Borkowski et al. is the fact that the observed N(Si IV) is about a factor of 20 larger than predicted for the young conduction front model discussed above. This model is by no means unique in underestimating the amount of observable Si IV (see Sembach & Savage 1992). A possible explanation is that the theoretical model neglects the additional production of ions caused by photoionization from the radiation emitted by the hot gas itself (Edgar & Chevalier 1986). Shapiro & Benjamin (1991, 1992) found that a very large enhancement in the Si IV column could result if the effects of self-photoionization were included for a one-dimensional flow of cooling gas (in the context of a Galactic fountain). We expect a similar effect would apply to the conductive interface.

6.3. *The Location of the Hot Gas Absorbing Near -26 km s^{-1}*

While we believe that the -26 km s^{-1} hot gas absorption is probably occurring in a conduction front (or fronts) of the type discussed above, the location of the absorption is much more difficult to determine owing to the complexity of the sight line. We believe there are two potential sites for the -26 km s^{-1} absorption: (1) at the edge of a stellar wind bubble plowing into the surrounding ambient interstellar medium, or (2) at the boundaries of the local diffuse interstellar clouds seen along the sight line. We favor the first of these as the most likely site and now discuss each in turn.

6.3.1. *Circumstellar Origin*

There is ample evidence that ζ Oph is interacting with surrounding interstellar material. Besides the H II region interactions discussed in § 5, ζ Oph has a fast stellar wind (Snow & Morton 1976) that must be modifying its immediate environment. Cirumstellar shells of swept-up interstellar material form around young stars with strong winds (Castor et al. 1975; Weaver et al. 1977), and it is on the inside edges of such shells that highly ionized atoms form between the cool shell material and the hot, shocked stellar wind. The radius (in parsecs) of a circumstellar shell in the "snowplow" phase is given by Castor et al. (1975) (see their eq. 6):

$$R_s(t) = 5.33 \times 10^{-3} \left[\frac{\dot{M} V_w^2}{n_0}\right]^{1/5} t^{3/5}\,, \tag{4a}$$

where $\dot{M}$ is the mass-loss rate of the star in solar masses per year, V_w is the terminal velocity of the wind in km s^{-1}, n_0 is the ambient interstellar density in cm^{-3}, and t is the age of the shock in years. For $\dot{M} = 6.3 \times 10^{-8}\ M_\odot$ yr^{-1}, $V_w = 1400$ km s^{-1} (Snow & Morton 1976; Howarth & Prinja 1989), and $n_0 = 4$ cm^{-3} (Reynolds 1988), we can rewrite equation (4a) as

$$R_s(t) = 2.66 \times 10^{-3}\, t^{3/5}\,. \tag{4b}$$

Differentiating with respect to time yields the velocity (in km s^{-1}) of the shock

$$\dot{R}_s(t) = 1560\, t^{-2/5}\,. \tag{5}$$

If the -26 km s^{-1} Si IV and C IV components seen toward ζ Oph arise at the inner boundary of the shell, we can solve equation (5) for the age of the shell. After accounting for the -13 km s^{-1} velocity of the expanding H II region (see § 5), we find an age for the shell of about 160,000 yr. Substituting the age into equation (4) yields a shell radius of 3.5 pc. The shell age is certainly much less than the age of the star but may be reasonable given that ζ Oph has such a large space velocity and may sample different interstellar conditions in this timescale. In 160,000 yr, ζ Oph moves 4.9 pc assuming a space velocity of 30 km s^{-1} (see Gull & Sofia 1979; Draine 1986). Therefore, the star will "outrun" the shell, and the ram pressure between the leading edge of the stellar wind bubble and the interstellar medium will determine the shape of the shell (Weaver et al. 1977; see their Fig. 7). Gull & Sofia (1979) obtained images of the faint [O III] emission surrounding ζ Oph and showed that a bow shock structure is present; they

also showed that the bow shock has a radius of curvature and apex direction consistent with the space velocity of the star.

The existence of a bow shock seen in [O III] emission is indirect evidence that the high ion absorption we have detected near -26 km s^{-1} may be occurring very near the star. Si IV should be present at locations where O III is observed since the two ions exist over such similar energy ranges (O III, 35.1–54.9 eV; Si IV, 33.5–45.1 eV). Models of shock heated gas interfaces of the type discussed above also predict corresponding C IV. Gull & Sofia (1979) found an angular extent of 45′ for the bow shock with a separation of 0.2 between the edge of the bow shock and the stellar disk. Although the angular extent of the emission leads to a shell radius considerably smaller than derived above from kinematical considerations, the extreme faintness of the [O III] emission probably results in a considerable underestimate for the overall bow shock size. It seems likely that at least some of the high ion absorption and [O III] emission are related, but until velocity measurements of the [O III] emission along the sight line are obtained, we cannot unambiguously attribute the Si IV and C IV absorption to the bow shock.

We can eliminate a general H II region interpretation for the -26 km s^{-1} high ion absorption due to the following consideration. (1) Depletion effects which are probably important in the H II region (see § 5) would lower the predicted high ion column densities well below the observed values. (2) The large widths of the high ion gas near -26 km s^{-1} require a turbulent velocity much larger than the turbulent velocity inferred for the H II region ($T \sim 7000$ K) gas discussed in § 5. (3) We find no direct evidence for H II region gas near -26 km s^{-1}. There is no detectable Al III absorption at this velocity, and although lower ionization states (Na I, Mg II, Si II, Fe II, Ca II) show some absorption near -26 km s^{-1}, the low ion profiles are much narrower than the broad high ion absorption (see Savage et al. 1992). Much of the low ion absorption near -26 km s^{-1} may arise in the local interstellar medium, but at least some must arise near the star if the stellar wind blown bubble model discussed above is correct. (4) We expect the high ion column densities resulting from Auger ionization of lower ionization species to be smaller than the observed values (see Cowie et al. 1981). If Auger ionization of C II and Si II into C IV and Si IV is the dominant process creating the high ion lines near -26 km s^{-1}, we expect the low and high ions would have similar velocity dispersions, a prediction in clear disagreement with the observations.

6.3.2. *Local Interstellar Origin*

Some of the broad absorption seen in the highly ionized species near -26 km s^{-1} may originate within the local interstellar medium (LISM). If the collisionally ionized gas is occurring in the LISM, then the observed Si IV and C IV absorption would provide further evidence that the solar neighborhood resides within a hot, low-density bubble of the type described by McCammon et al. (1983).

The similarity of the hot gas velocity centroids and the velocity of a diffuse, neutral cloud complex centered at -26 km s^{-1} supports the idea of a common origin for these features. The low ion absorption at -26 km s^{-1} consists of at least two-components centered near -26.7 and -25.5 km s^{-1} (Hobbs 1969). The local origin ($d < 60$ pc) of the diffuse clouds absorbing near -26 km s^{-1} has been established by Frisch & York (1984) through detections of Na I absorption near -26 km s^{-1} toward three nearby stars (55–90 pc) situated within 2° of the ζ Oph sight line. The -26 km s^{-1} absorption, identified as component S in the H I 21 cm study made by Cappa de Nicolau & Poppel (1986), has a large angular extent.

Conduction fronts of the type discussed in § 6.2 at the boundaries of these cool clouds could account for the observed high ion absorption. For instance, a satisfactory picture is the predicted outcome for two conduction zones (on the front and rear of a cool cloud embedded in hot gas) with inclination angles whose secants are about 2 and a reduction of the carbon abundance to a factor of 3 below the cosmic value (see § 5.3). Frisch (1981) found that nearby gas in this general direction has been shock processed, and she hypothesized that the explosive event which created Radio Loop I may have processed material as it flooded into the solar neighborhood. The same event may be responsible for the large peculiar velocity of ζ Oph; the star could have been ejected from the center of the Sco-Cen Association (Berkhuijsen et al. 1971; see also Glaspey 1972). Berkhuijsen et al. predicted an expansion velocity of 25 km s^{-1} for the resulting shell, in good agreement with the observed velocity centroids of the high ions and neutral cloud complex absorption. However, the estimated age of 2×10^6 yr for the event is considerably older than the age of the conduction front we prefer as the source for the observed high ion absorption. X-ray observations indicate that a more recent event, perhaps the one that created Radio Loop IV, has probably reheated the interior of the Loop I bubble (Iwan 1980), and therefore a local origin for the gas cannot be dismissed.

7. C IV ABSORPTION AT -61 km s^{-1}

We detect C IV absorption at $v = -61.0 \pm 9.4$ km s^{-1} that is not detected in the other species. We find $b = 12.8 \pm 8.0$ km s^{-1} and $\log N(\mathrm{C\ IV}) = 12.19 \pm {}^{0.23}_{0.54}$ (see Table 4) for this absorption. If it arises in an environment similar to the one producing the high ion absorption near -26 km s^{-1}, we would expect the Si IV column density [$\log N(\mathrm{Si\ IV}) \approx 11.28$; $W_\lambda(1393) \approx 1.7$ mÅ] to be near our detection threshold [$\log N < 11.3$ (2 σ) for $-70 \le v \le -50$ km s^{-1}]. There is little evidence for neutral or weakly ionized species at these velocities; the strong N I λλ1200.223, 1200.710 and Fe II λ2600.163 lines show no evidence for absorption at $v < -40$ km s^{-1} [$\log N(\mathrm{N\ I}) < 11.8$ (2 σ) and $\log N(\mathrm{Fe\ II}) < 10.8$ (2 σ) for $-70 \le v \le -50$ km s^{-1}]. Therefore, an origin in a warm-hot gas interface can be ruled out.

For reasons similar to those in § 6.3, it is unlikely that the C IV absorption arises from Auger ionization of C II in the general H II region around the star. However, that discussion does not preclude the formation of the feature by similar processes in the stellar wind. High ion narrow absorption line components (NACs) created in developed stellar winds around young stars are quite common; they are found in more than 80% of O and B star wind spectra (Howarth & Prinja 1989). NACs observed in the ζ Oph spectrum are concentrated at large negative velocities (one group at -1385 km s^{-1}, one group at -1250 km s^{-1}) and tend to be long-lived (Howarth, Prinja, & Willis 1984). Weak features and continuum distortions can later become observable NACs and may be created by episodic mass-loss events or optical depth enhancements in corotating interacting regions in stellar winds (Howarth 1984; Mullan 1984, 1986). ζ Oph undergoes periodic mass-loss disturbances (Barker & Brown 1974; Irvine 1974; Ebbets 1981) that may give rise to the -61 km s^{-1} absorption. Bjorkman & Cassinelli (1993) have found that highly ionized gas is produced by standing shocks that heat forming equatorial disks

around rapidly rotating stars. These shocks collisionally ionize the gas to $T \approx 10^5$ K for stellar rotational speeds of ≈ 300 km s^{-1} and can produce observable amounts of C IV. Further observations of the -61 km s^{-1} C IV feature are needed to determine if this is a viable explanation for the observed absorption.

8. CONCLUSIONS AND FUTURE PROSPECTS

To help summarize the physical properties of the different regions along the ζ Oph sight line, we have listed the general properties of the regions in Table 5. The main observational results and conclusions resulting from our GHRS 3.5 km s^{-1} resolution observations of the highly ionized gas toward ζ Oph are as follows.

1. The Si IV profiles exhibit narrow ($b = 5.3$ km s^{-1}) absorption centered on $v = -15$ km s^{-1}. No correspondingly narrow C IV component is seen at this velocity. The simplest explanation for the origin of the Si IV absorption is that is arises from photoionization within the H II region surrounding ζ Oph.

2. Predictions of the amount of Si IV and C IV expected in the H II region surrounding ζ Oph (Cowie et al. 1981) overestimate the amount of absorption by a factor of 30 for Si IV and a factor of more than 10 for C IV. Some of the differences between the observed and predicted column densities can be explained if the elemental abundances of silicon and carbon are below their solar value by amounts typically seen in the ISM where dust has not been heavily processed. The presence of a stellar wind may also contribute to some of the differences.

3. The Al III profile exhibits narrow ($b = 4.3$ km s^{-1}) absorption centered on $v = -8$ km s^{-1} which is displaced 7 km s^{-1} from the strong Si IV absorption. H II region models that include the effects of expansion can account for the observed magnitude and direction of the velocity offset between the Al III and Si IV profiles. A weaker Al III component centered near the main Si IV absorption at $v = -15$ km s^{-1} probably arises in the Si IV–bearing gas.

4. The Si IV and C IV profiles exhibit a broad ($b = 15$ to 18 km s^{-1}), weak absorption centered on $v \approx -26$ km s^{-1}. This absorption is not detected in the N V lines. The Si IV and C IV absorption may arise in a conductive interface on the inner edge of the expanding shell of the stellar wind bubble surrounding ζ Oph. Alternatively, the absorption may arise in a pair of young conduction fronts on the front and rear of a cool cloud embedded in a hot gas in the local interstellar medium. The existence of a bow shock observed around ζ Oph in [O III] emission (Gull & Sofia 1979) and the stellar bubble parameters calculated in § 6.3.1 lead us to favor the former of these two interpretations. In either case, the observed ionic ratios and widths of the lines favor formation in a conduction front (or fronts) in an early stage of development ($t \leq 10^5$ yr).

5. We have derived a new upper limit to the amount of O VI along the sight line [log N(O VI) ≤ 12.69; see Appendix] from *Copernicus* satellite archival data. The observed upper limit to N(O VI) lends further credence to the conclusions based upon the GHRS results given in conclusion 4.

6. We observe weak C IV absorption centered near -61 km s^{-1}. No detectable absorption is present in other species at this velocity. The absorption may arise near the base of the stellar wind in material heated by standing shocks caused by the rapid rotation of the star.

7. The Si IV and C IV profiles differ from the profiles of lower ionization species such as Mg II. The high ion profiles are much broader than the narrow low ion profiles. The narrowest Si IV feature has $b = 5.3$ km s^{-1}; the Mg II feature near -15 km s^{-1} is narrower with $b = 2.2$ km s^{-1}. The C IV absorption near -61 km s^{-1} has no detectable counterpart in the low ion lines. Our favored interpretation for the broad -26 km s^{-1} broad high ion absorption line (see conclusion 4 and 5) requires that some of the low and high ion absorption be associated, although the two types of species certainly arise in different physical environments.

The interpretation of the features discussed in this paper

TABLE 5

GENERAL PROPERTIES OF THE ζ OPH SIGHT LINE[a]

Region	$\langle v \rangle$ (km s^{-1})	d (pc)	T (K)	n_e (cm^{-3})	References
Diffuse clouds[b]	-15	>100	56	0.063	
Diffuse clouds	-26	>60	<5500	<0.093	1
H II region[c]	-13	Circumstellar	7000	4.0	2
Wind/ISM interface[d]	-26?	Circumstellar	Shocked	?	3
Bow shock[e]	?	Circumstellar	Shocked	?	4, 5

[a] General properties of the different regions along the ζ Oph sight line. See text for details and additional references.

[b] Only the -15 km s^{-1} diffuse cloud in molecular lines. Gas phase depletions are more severe in the -15 km s^{-1} cloud than the -26 km s^{-1} cloud, and it is clear that the -26 km s^{-1} cloud is more ionized than the -15 km s^{-1} cloud. It is possible that some of the broad -26 km s^{-1} high ion absorption may arise in interface associated with the -26 km s^{-1} local diffuse cloud and a very hot surrounding medium.

[c] The -15 km s^{-1} Si IV absorption and -8 km s^{-1} Al III absorption arise within the H II region. The physical conditions within the Strömgren radii containing these species may differ greatly from the values listed in the table (see § 5). For a discussion of the interaction of the H II region on the surrounding medium, see Draine 1986.

[d] Some of the -26 km s^{-1} high ion absorption may be associated with this region. Much of the interior of such a bubble would be too hot to detect in Si IV or C IV, therefore, the detected lines at -26 km s^{-1} presumably arise at the interface between the wind-blown bubble and surrounding ISM. The temperature of the gas bearing the C IV and Si IV ions is likely to be near 10^5 K.

[e] The bow shock is seen in IR dust emission (60 μm, 100 μm), [O III] emission, and Hα emission. This region may be related to the wind-blown bubble region discussed in footnote *d*.

REFERENCES.—(1) Savage et al. 1992; (2) Reynolds 1988; (3) this paper, § 6; (4) Gull & Sofia (1979); (5) Van Buren & McCray 1988.

would benefit greatly from repeated high-dispersion observations of the high ion UV lines. In particular, additional measurements of the broad high ion features at -26 km s^{-1} and -61 km s^{-1} would provide information about the stability of these absorptions over time. Detection of Si IV and C IV absorption at -26 km s^{-1} in the spectra of other nearby stars in the direction of ζ Oph would favor a local origin for the gas if the conductive interface interpretation is correct and would provide evidence for hot gas in the local interstellar medium. The observations could even be obtained with the GHRS first-order gratings using the SSA to preserve the G160M spectral resolution, provided data having the quality of the Si IV spectra shown in Figure 2 could be obtained. Higher S/N echelle spectra would be useful for searching for low-velocity wind features. Finally, velocity measurements of the optical [O III] emission would be helpful in determining the bow shock velocity and whether or not the [O III] emission and high ion absorption are related.

We thank U. J. Sofia for providing reduced versions of the N I and Fe II spectra used to estimate column density limits on the neutral gas near -61 km s^{-1}. We thank J. Raymond and L. Spitzer, Jr. for useful comments on some of the material presented in this paper. We appreciate helpful suggestions from the anonymous referee. K. R. S. acknowledges support from a Hubble Fellowship provided by NASA through grant HF-1038.01-92A from the Space Telescope Science Institute, which is operated by AURA under NASA contract NAS5-26555. B. D. S. recognizes support from NASA grant NAS5-29368. E. B. J. acknowledges support from NASA grant NAG5-1714 to Princeton University.

APPENDIX

A NEW DETERMINATION OF AN UPPER LIMIT FOR N(O VI) FROM *COPERNICUS* DATA

A fundamental problem in detecting UV absorptions from O VI is that the strongest member of the doublet, the line at 1031.926 Å, usually has interference from the 6–0 $R(0)$ line of the Lyman band of HD at 1031.912 Å (Jenkins 1978a). Thus, to determine N(O VI) one must either look at the strong line and subtract out the influence of the HD feature or rely entirely on the weaker member of the multiplet at 1037.617 Å. The latter tactic was employed by Morton (1975) in his analysis of the far-UV spectrum of ζ Oph recorded by *Copernicus*. Unfortunately, the ζ Oph sight line contains an unusually large column density of H_2, and, consequently, measurements are weakened by a significant suppression of the continuum flux by the wings of the very strong 5–0 $R(1)$ and $P(1)$ lines of H_2 that are centered at 1037.15 and 1038.16 Å, respectively. Morton's measurements showing that log N(O VI) < 13.38, the only determination published to date, is based on an upper limit of 11 mÅ for the equivalent width of the 1037.617 Å feature seen in a single scan.

In a later paper, Wright & Morton (1979) reported on an intensive study of the HD lines in the spectrum of ζ Oph. We can make use of information given in that article to derive a significantly more sensitive determination for N(O VI) than Morton's earlier result. Precise information on the column density of HD in the lowest rotation level given by Wright & Morton (1979) allows us to gauge well the expected interference on top of a possible 1032 Å feature of O VI. In addition, the paper lists a good measurement of the equivalent width of this feature, based on a total of 15 scans, which represents a large improvement in precision over that of the earlier study.

To interpret a blend of a possible O VI feature with one that is known to come from HD, we must resort to a model for the velocity widths and relative placement of the two features. Wright & Morton assumed the b value for HD was 3.8 km s^{-1}, based on the results of Spitzer, Cochran, & Hirshfeld (1974) for H_2 in rotational levels $J = 3$ to 6. While it is not absolutely certain that HD and H_2 have the same b values, Wright & Morton claim that b outside the range 2.5 to 6.5 km s^{-1} would have produced relative equivalent widths of the 6–0 and 3–0 lines that were inconsistent with the observations. After considering our results for C IV and Si IV, we believe that is unlikely that the b value of O VI could be lower than 10 km s^{-1}. We will adopt this value for our model. It should be obvious that this assumed number is very important for the outcome; in principle, N(O VI) could be arbitrarily large if its absorption could hide completely inside the moderately saturated HD line. For the relative placement of the HD and O VI lines, a most conservative position for deriving an upper limit to N(O VI) is to assume that the features are exactly lined up in central wavelength. The 0.014 Å difference in laboratory wavelengths between the O VI and HD features corresponds to a Doppler shift of 4 km s^{-1}. Assuming that the HD absorption is centered on the velocity of the principal diffuse cloud complex toward ζ Oph near $v = -15$ km s^{-1}, this conservative limit will refer to an O VI velocity $v = -19$ km s^{-1}.

Wright & Morton reported a nominal log N(HD) = 14.26, based on their analysis of five different lines from the $J = 0$ level. This column density should give $W_\lambda = 23.5$ mA for the 6–0 $R(0)$ line if $b = 3.8$ km s^{-1}. This expectation for W_λ is very close to the observed value of 23.2 ± 1.2 mÅ. There is additional evidence to support the viewpoint that HD is responsible for virtually all of the absorption: one of us (E. B. J.) found a plot of the summed scans in the *Copernicus* data archive and measured the width of the feature to be 55 mÅ (FWHM), only slightly larger than the spectrograph instrumental profile width of 51 mÅ (Spitzer & Morton 1976).

To obtain an upper limit for the presence of some very weak contributon by O VI at the same wavelength, we assume that the true column density of HD is at Wright & Morton's $-2\,\sigma$ error limit, log N(HD) = 14.20. We find that to obtain a composite feature at the $+2\,\sigma$ measurement error limit for W_λ, 25.6 mA, we would need log N(O VI) = 12.69 near $v = -19$ km s^{-1} if the velocity model discussed earlier applies. This number, expressed as an upper limit, is the one that we shall adopt for our interpretation of the properties of broad absorption features caused by hot gas toward ζ Oph. If the O VI line is well removed in velocity from the HD feature, the upper limit decreases to log N(O VI) = 12.50. This smaller upper limit, for example, applies to possible O VI absorption near $v = -61$ km s^{-1}.

REFERENCES

Aannstad, P. A. 1973, in IAU Colloq. 52, Insterstellar Dust and Related Topics, ed. J. Mayo Greenberg & H. C. van de Hulst (Dordrecht: Reidel), 341
Aldrovandi, S. M., & Pequignot, D. 1973, A&A, 25, 137
Barker, P. K., & Brown, T. 1974, ApJ, 192, L11
Barker, E. S., Lugger, P. M., Weiler, E. J., & York, D. G. 1984, ApJ, 280, 600
Beckenstein, J. D., & Bowers, R. L. 1974, ApJ, 190, 653
Beckhuijsen, E. M., Haslam, C. G. T., & Salter, C. J. 1971, A&A, 14, 252
Bjorkman, J. E., & Cassinelli, J. P. 1993, Wisconsin Astrophysics Preprint 450
Blaauw, A. 1961, Bull. Astron. Inst. Netherlands, 15, 265
Black, J. H., & Dalgarno, A. 1977, ApJS, 34, 405
Black, J. H., Dupree, A. K., Hartmann, L. W., & Raymond, J. C. 1980, ApJ, 239, 502
Blint, R. J., Watson, W. D., & Christensen, R. B. 1976, ApJ, 205, 634
Borkowski, K. J., Balbus, S. A., & Fristrom, C. C. 1990, ApJ, 355, 501
Cappa de Nicolau, C. E., & Poppel, W. G. L. 1986, A&A, 164, 274
Cardelli, J. A., Ebbets, D. C., & Savage, B. D. 1990, ApJ, 365, 789
Cardelli, J. A., Mathis, J. S., Ebbets, D. C., & Savage, B. D. 1993, ApJ, submitted
Cardelli, J. A., et al. 1991, ApJ, 377, L57
Castor, J. C., McCray, R., & Weaver, R. 1975, ApJ, 200, L107
Christensen, R. B., Watson, W. D., & Blint, R. J. 1977, ApJ, 213, 712
Code, A. D., Davis, J., Bless, R. C., & Brown, R. H. 1976, ApJ, 203, 417
Conti, P. S., & Ebbets, D. 1977, ApJ, 213, 438
Cowie, L. L., Jenkins, E. B., Songaila, A., & York, D. G. 1979, ApJ, 232, 467
Cowie, L. L., & McKee, C. F. 1977, ApJ, 211, 135
Cowie, L. L., & Songaila, A. 1986, ARA&A, 24, 499
Cowie, L. L., Taylor, W., & York, D. G. 1981, ApJ, 248, 528
Cox, D. P., & Smith, B. W. 1974, ApJ, 189, L105
Crutcher, R. M. 1977, ApJ, 217, L109
———. 1979, ApJ, 231, L157
de Boer, K. S., & Morton, D. C. 1979, A&A, 71, 141
de Geus, E. J., & Burton, W. B. 1991, A&A, 246, 559
de Kool, M., & de Jong, T. 1985, A&A, 149, 151
Draine, B. T. 1986, ApJ, 310, 408
Duncan, D. K. 1992, Goddard High-Resolution Spctrograph Instrument Handbook, Version 3.0 (STScI)
Duncan, D. K., & Ebbets, D. C. 1990, Goddard High-Resolution Spectrograph Instrument Handbook, Version 2.1 (STScI)
Dupree, A. K., & Raymond, J. C. 1983, ApJ, 275, L71
Ebbets, D. C. 1981, PASP, 93, 119
Edgar, R. J., & Chevalier, R. A. 1986, ApJ, 310, L27
Elitzur, M., & Watson, W. D. 1978a, ApJ, 222, L141
———. 1978b, ApJ, 226, 457
———. 1980, ApJ, 236, 172
Federman, S. R., Sheffer, Y., Lambert, D. L., & Gilliland, R. L. 1993, ApJ, 314, L51
Frisch, P. C. 1981, Nature, 293, 377
Frisch, P. C., & York, D. G. 1984, in IAU Colloq. 81, The Local Interstellar Medium, ed. Y. Kondo, F. C. Bruhweiler, & B. D. Savage (NASA CP2345), 113
Georgelin, Y. P., & Georgelin, Y. M. 1970, A&A, 166, 225
Glaspey, J. W. 1972, AJ, 77, 474
Gull, T. R., & Sofia, S. 1979, ApJ, 230, 782
Hobbs, L. M. 1969, ApJ, 157, 135
———. 1973a, ApJ, 180, L79
———. 1973b, ApJ, 181, 79
Hollenbach, D., Chu, S., & McCray, R. 1976, ApJ, 208, 458
Howarth, I. D. 1984, MNRAS, 206, 625
Howarth, I. D., & Prinja, R. K. 1989, ApJS, 69, 527
Howarth, I. D., Prinja, R. K., & Willis, A. J. 1984, MNRAS, 208, 525
Irvine, N. J. 1974, ApJ, 188, L19
Isberg, B. 1968, Ark. Fys., 35, 551
Iwan, D. 1980, ApJ, 239, 316
Jenkins, E. B. 1978a, ApJ, 219, 845
———. 1978b, ApJ, 220, 107
———. 1987, in Interstellar Processes, ed. D. J. Hollenbach & H. A. Thronson (Dordrecht: Reidel), 533
Joshi, P., & Tarafdar, S. P. 1975, Ap&SS, 36, 281
Jura, M. 1975, ApJ, 197, 581
Kafatos, M. 1973, ApJ, 182, 433
Kambe, E., Ando, H., & Hirata, R. 1990, PASJ, 42, 687
Kurucz, R. L. 1979, ApJS, 40, 1
Liszt, H. 1992, ApJ, 390, 226
Lucy, L. B. 1983, ApJ, 274, 372
MacLow, M. M., Van Buren, D., Wood, D. O., & Churchwell, E. 1991, ApJ, 369, 395
Marschall, L. A., & Hobbs, L. M. 1972, ApJ, 173, 43
Martin, W. C., & Zalubas, R. J. Phys. Chem. Ref. Data, 12, 323
McCammon, D., Burrows, D. N., Sanders, W. T., & Krauhaar, W. L. 1983, ApJ, 269, 107
McCray, R., & Snow, T. P. 1979, ARA&A, 17, 213
McKee, C. F., & Cowie, L. L. 1977, ApJ, 215, 213
McKee, C. F., & Ostriker, J. P. 1977, ApJ, 218, 148
Monteiro, T. S., Flower, D. R., Pineau des Forêts, G., & Roueff, E. 1988, MNRAS, 234, 863
Morton, D. C. 1975, ApJ, 197, 85
———. 1976, ApJ, 203, 386
———. 1991, ApJS, 77, 119
Mullan, D. J. 1984, ApJ, 283, 303
———. 1986, A&A, 165, 157
Osterbrock, D. E. 1989, Astrophysics of Gaseous Nebulae and Active Galactic Nuclei (Mill Valley: University Science Books)
Pwa, T. H., & Pottasch, S. R. 1986, A&A, 164, 116
Reynolds, R. J. 1988, ApJ, 333, 341
Reynolds, R. J., & Ogden, P. M. 1982, AJ, 87, 306
Sarazin, C. L. 1976, ApJ, 208, 323
———. 1977, ApJ, 211, 772
Savage, B. D., et al. 1991, ApJ, 377, L54
Savage, B. D., Cardelli, J. A., & Sofia, U. J. 1992, ApJ, 401, 706
Savage, B. D., & Sembach, K. R. 1991, ApJ, 379, 245
Sembach, K. R., Danks, A., & Savage, B. D. 1993, A&AS, 100, 107
Sembach, K. R., & Savage, B. D. 1992, ApJS, 83, 147
Shapiro, P. R., & Benjamin, R. A. 1991, PASP, 103, 923
———. 1992, in Star-Forming Galaxies and Their Interstellar Media, ed. J. J. Franco (New York: Cambridge Univ. Press)
Shapiro, P. R., & Moore, R. T. 1976, ApJ, 207, 460
Shull, J. M., & Van Steenberg, M. 1982, ApJS, 48, 95
Slettebak, A. 1966, ApJ, 145, 126
Smith, B. W. 1977, ApJ, 211, 404
Snow, T. P., & Morton, D. C. 1976, ApJS, 32, 429
Spitzer, L., Jr. 1978, Physical Processes in the Interstellar Medium (New York: Wiley)
———. 1990, ARA&A, 28, 71
Spitzer, L., Jr., Cochran, W. D., & Hirshfeld, A. 1974, ApJS, 28, 373
Spitzer, L., Jr., & Jenkins, E. B. 1975, ARA&A, 13, 133
Spitzer, L., Jr., & Morton, W. A. 1976, ApJ, 204, 731
Van Buren, D., MacLow, M. M., Wood, D. O., & Churchwell, E. 1990, ApJ, 353, 570
Van Buren, D., & McCray, R. 1988, ApJ, 329, L93
Van Steenberg, M. E., & Shull, J. M. 1988, ApJ, 330, 942
Vogt, S. S., & Penrod, G. D. 1983, ApJ, 275, 661
Walker, G. A. H., Yang, S., & Fahlman, G. G. 1979, ApJ, 233, 199
Weaver, R. McCray, R., Castor, J., Shapiro, P., & Moore, R. 1977, ApJ, 218, 377
Wright, E. L., & Morton, D. C. 1979, ApJ, 227, 483